On the Response of a Nonlinear Structure to High Kurtosis Non-Gaussian Random Loadings

Stephen A. Rizzi[1], Adam Przekop[2], Travis Turner[1]
[1]Structural Acoustics Branch, NASA Langley Research Center, Hampton, Virginia 23681, USA
[2]Analytical Services and Materials, Inc., Hampton, Virginia 23666, USA
email: Stephen.A.Rizzi@nasa.gov, Adam.Przekop@nasa.gov, Travis.L.Turner@nasa.gov

ABSTRACT: This paper is a follow-on to recent work by the authors in which the response and high-cycle fatigue of a nonlinear structure subject to non-Gaussian loadings was found to vary markedly depending on the nature of the loading. There it was found that a non-Gaussian loading having a steady rate of short-duration, high-excursion peaks produced essentially the same response as would have been incurred by a Gaussian loading. In contrast, a non-Gaussian loading having the same kurtosis, but with bursts of high-excursion peaks was found to elicit a much greater response. This work is meant to answer the question of when consideration of a loading probability distribution other than Gaussian is important. The approach entailed nonlinear numerical simulation of a beam structure under Gaussian and non-Gaussian random excitations. Whether the structure responded in a Gaussian or non-Gaussian manner was determined by adherence to, or violations of, the Central Limit Theorem. Over a practical range of damping, it was found that the linear response to a non-Gaussian loading was Gaussian when the period of the system impulse response is much greater than the rate of peaks in the loading. Lower damping reduced the kurtosis, but only when the linear response was non-Gaussian. In the nonlinear regime, the response was found to be non-Gaussian for all loadings. The effect of a spring-hardening type of nonlinearity was found to limit extreme values and thereby lower the kurtosis relative to the linear response regime. In this case, lower damping gave rise to greater nonlinearity, resulting in lower kurtosis than a higher level of damping.

KEY WORDS: Nonlinear structural dynamics; Non-Gaussian random loading; Damping.

1 INTRODUCTION

High performance aircraft structures subject to extreme thermal-acoustic loadings may exhibit geometric and material nonlinearity. These nonlinearities alter the dynamic stress response which in turn affects the high-cycle fatigue life. Recent work by the authors investigated the high-cycle fatigue of a nonlinear aluminum structure undergoing snap-through response in a thermally post-buckled condition under Gaussian [1] and a non-Gaussian loading with temporal characteristics similar to those found in turbulent boundary layer (TBL) pressure fluctuations [2, 3]. In the latter work, it was found that such non-Gaussian loadings, with high and steady rates of peak excursions, produced nearly Gaussian responses in the pre-buckled linear response regime. In the pre- and post-buckled nonlinear response regime, the effects of geometric and material nonlinearity were more important than the loading probability distribution. Consequently, fatigue life estimates for Gaussian and non-Gaussian loadings were comparable and well within customarily applied margins for loading uncertainty and variances between damage models. The response and fatigue was additionally investigated by considering a second form of non-Gaussian loading, having similar kurtosis to the TBL-like loading, but with long bursts of high amplitude excursions. This loading resulted in a significantly reduced fatigue life compared to the Gaussian case. Indeed, the question of when consideration of the loading probability distribution is necessary is at the heart of this study.

To that end, this paper further explores the dependency of the linear and geometrically nonlinear dynamic response of an aluminum beam structure on the distribution of three random loadings; a Gaussian loading, a non-Gaussian loading having a steady distribution of peak excursions, and a non-Gaussian loading with bursts of high amplitude excursions. The Central Limit Theorem (CLT) [4] is used to determine when the response is Gaussian through consideration of loading timescales relative to the period of the system impulse response, and the nonlinearity in the system. The effect of damping is considered for linear and nonlinear responses having Gaussian and non-Gaussian distributions. Response time histories are examined to help determine the circumstances under which the response becomes non-Gaussian. The relevance of this work to high kurtosis random vibration testing is additionally discussed.

2 GAUSSIAN AND NON-GAUSSIAN RANDOM PROCESSES

A random variable x is said to be Gaussian if its probability density function (PDF) is given by

$$p(x) = \frac{1}{\sqrt{2\pi\sigma^2}} e^{-\frac{(x-m)^2}{2\sigma^2}} \tag{1}$$

where m is the mean and σ is the standard deviation. The variance σ^2 is the second central moment of $p(x)$, namely M_2. For discrete time series data, the central moments and mean m are computed from

$$M_j = \frac{1}{n}\sum_{i=1}^{n} [\, x_i - m \,]^j, \qquad m = \frac{1}{n}\sum_{i=1}^{n} x_i \tag{2}$$

where n is the number of points in the sample time history record. The probability distribution, or cumulative distribution function (CDF) is written as

$$P(x) = \sum_{x_j \le x} p(x_j) . \tag{3}$$

The fact that probability distributions of many physical processes are Gaussian can be partially explained by the CLT. Let $x_1, x_2, \ldots, x_N$ be a set of N real-valued random variables such that:

i. x_i (i=1, 2, …, N) are mutually independent,

ii. $P(x_i)$ are unspecified and may be different, and

iii. m and σ exist for each vector x_i.

Define the sum random variable χ as

$$\chi = \sum_{i=1}^{N} h_i x_i \tag{4}$$

where h_i are arbitrary fixed constants. Then, according to the CLT, the sum random variable will be normally distributed as $N \to \infty$ provided that the sum is not heavily weighted by a small number of terms $h_i x_i$. Let the component random variables be constructed as:

$$x_i = \begin{Bmatrix} f_1(t_i) \\ f_2(t_i) \\ \vdots \\ f_K(t_i) \end{Bmatrix} \tag{5}$$

where $f_1(t), f_2(t), \cdots, f_K(t)$ are an ensemble of K loading time histories. The sum random variable may then be written as

$$\begin{Bmatrix} \chi_1 \\ \chi_2 \\ \vdots \\ \chi_K \end{Bmatrix} = \sum_{i=1}^{N} h_i \begin{Bmatrix} f_1(t_i) \\ f_2(t_i) \\ \vdots \\ f_K(t_i) \end{Bmatrix} . \tag{6}$$

Via time domain convolution, the elements of the sum random variable form the displacement time history when the constants h are the system impulse response function and each successive loading time history is indexed by 1, that is,

$$\begin{Bmatrix} \chi_1 \\ \chi_2 \\ \vdots \\ \chi_K \end{Bmatrix} = \tag{7}$$

$$\begin{Bmatrix} h_1 f(t_L) & + & h_2 f(t_{L-1}) & + & \cdots & + & h_L f(t_1) \\ h_1 f(t_{L+1}) & + & h_2 f(t_L) & + & \cdots & + & h_L f(t_2) \\ & & & \vdots & & & \\ h_1 f(t_{L+K}) & + & h_2 f(t_{L+K-1}) & + & \cdots & + & h_L f(t_K) \end{Bmatrix}$$

where L is the period of the impulse response function. Thus, the CLT can be used to determine under what circumstances the probability distribution of the displacement (the sum random variable) is Gaussian.

The principal metrics describing non-Gaussian features of the PDF are skewness λ and kurtosis γ, which may be expressed in terms of the central moments as:

$$\lambda = \frac{M_3}{(M_2)^{3/2}} = \frac{M_3}{\sigma^3}, \qquad \gamma = \frac{M_4}{(M_2)^2} = \frac{M_4}{\sigma^4} . \tag{8}$$

The kurtosis characterizes the sharpness of the PDF peak and the width of the PDF tails. The skewness is a measure of the asymmetry of the PDF. For a Gaussian distribution, $\lambda = 0$ and $\gamma = 3$. A kurtosis value greater than 3 indicates a sharper peak and wider tails relative to a Gaussian distribution.

Another indicator of non-Gaussian character is the crest factor C, defined by

$$C = |x|_{peak} / x_{rms} . \tag{9}$$

In contrast to the skewness and kurtosis, no strict theoretical value can be defined for the crest factor of a non-Gaussian process because the magnitude of the largest peak depends on the length of time history. While the skewness and kurtosis summarize the effect of all peaks that make a signal non-Gaussian, the crest factor takes into account only the largest peak.

3 NONLINEAR DYNAMIC RESPONSE SIMULATION

3.1 Finite Element Model

An aluminum beam structure previously considered [1, 2] served as the basis for the current investigation. The beam was chosen so that long duration nonlinear simulations would be practical. The beam measured 457.2 mm x 25.40 mm x 2.286 mm (l x w x h) and had clamped boundary conditions at both ends. The material properties used were: elastic modulus E = 73.11 GPa, shear modulus G = 27.59 GPa, and mass density = 2763 kg/m^3. Mass proportional damping was specified according to the relation

$$c = 2\zeta\omega \tag{10}$$

where c is the mass-proportional damping constant, ζ is the viscous damping factor, and ω is the circular frequency. Two levels of damping, spanning a practical range, were considered in this study. Values of c were 14.52 s^{-1} and 1.82 s^{-1}, corresponding to viscous damping factors of 2% and 0.25%, respectively, at the linear fundamental frequency of 57.8 Hz.

The beam response was analyzed with the finite element code ABAQUS [5]. The finite element model consisted of 144 B21 beam elements 3.175 mm long. The two-node B21 element allows single-plane bending and has one rotational and two translational degrees-of-freedom (DoF) at each node. The clamped boundary conditions were modeled by constraining the rotational and both translational (transverse and in-plane) DoFs at each end of the beam.

The ABAQUS/Explicit solution was used with an automatic time step adjustment, known as ‘element-by-element’ in ABAQUS. This approach yields a conservative time step increment. Nodal displacement time histories were computed for each loading condition. Transverse displacements at the half-span node are subsequently shown. All simulations were performed at ambient temperature conditions.

3.2 *Acoustic Loading*

Two different types of non-Gaussian loadings with high kurtosis were considered in this paper. One was generated to resemble the temporal characteristics of a turbulent boundary layer (TBL) fluctuating pressure loading [3]. This loading type had a steady rate of high-excursion peaks and is subsequently referred to as *steady non-Gaussian*. The other loading type considered had bursts of high-excursion peaks and is subsequently referred to as *burst non-Gaussian*. A Gaussian loading was additionally considered for comparison. The same nominal kurtosis was chosen for both non-Gaussian loading types, namely $\gamma = 7$. The effect of skewness was not investigated in this study, hence skewness was nominally zero. Details of the load generation procedure are discussed in references [2, 6]. The method of load generation does not permit skewness and kurtosis to be specified precisely, so actual values of skewness, kurtosis and crest factor of the generated loadings are provided in Table 1. All loadings were normalized to a standard deviation of 1.

Table 1. Skewness, kurtosis and crest factor of three generated loadings.

Loading Type	Skewness λ	Kurtosis γ	Crest Factor C
Gaussian	$4.9\text{x}10^{-3}$	2.99	4.83
Steady	$7.2\text{x}10^{-3}$	7.11	7.40
Burst	$-1.9\text{x}10^{-2}$	6.88	9.21

An identical flat spectral distribution between 1–1500 Hz was specified for each Gaussian and non-Gaussian loading. The generated loadings were scaled to an overall sound pressure level of 104 dB (re: 20 µPa) to study the beam response in the linear regime, and to 152 dB to study the geometrically nonlinear (large deflection) response. Note that the response due to the 152 dB loading was previously found to remain in the linear elastic regime [1]. The loading was spatially uniform for both the linear and nonlinear response regimes. Simulations of 104 s were run for the Gaussian and steady non-Gaussian loadings, and simulations of 208 s were run for the burst non-Gaussian loadings. These simulation times were based on convergence of high-cycle fatigue life predictions in the earlier work [2]. The first 1 s of simulated random response was removed in each case to minimize the effect of transient behavior on the calculated statistics. Power spectral density (PSD) estimates were made using a 32,768 point transform giving a frequency resolution of 0.61 Hz.

It is clear from the long sample time histories shown in Figure 1 that specification of the skewness, kurtosis and spectral distribution is insufficient to uniquely define the loading. Although each normalized loading time history has the same unity standard deviation, the non-Gaussian loadings have greater peak values, as indicated by their crest factors in Table 1 and their PDFs shown in Figure 2. Turning points are the sequence of local extremes (minima and maxima) and were computed as a function of time to help quantify the unsteadiness in the loadings. Turning points are often used to compute rainflow cycles for use in fatigue life predictions [7]. As shown in Figure 3, the time histories of the number of turning points in excess of 3σ for non-overlapping 1 s blocks indicate a near steady rate of roughly 20 per second for the Gaussian loading and 50 per second for the steady non-Gaussian loading. In contrast, the number of turning points per second varies significantly for the burst non-Gaussian loading, ranging from 0 to over 600 per second.

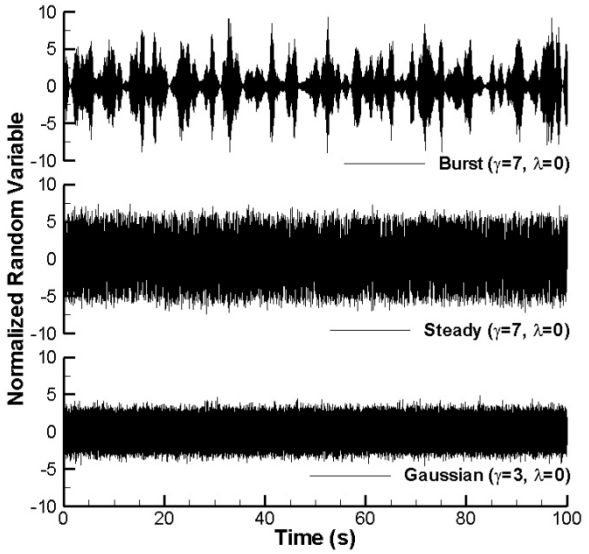

Figure 1. Long sample time histories of simulated Gaussian, and steady and burst non-Gaussian loadings.

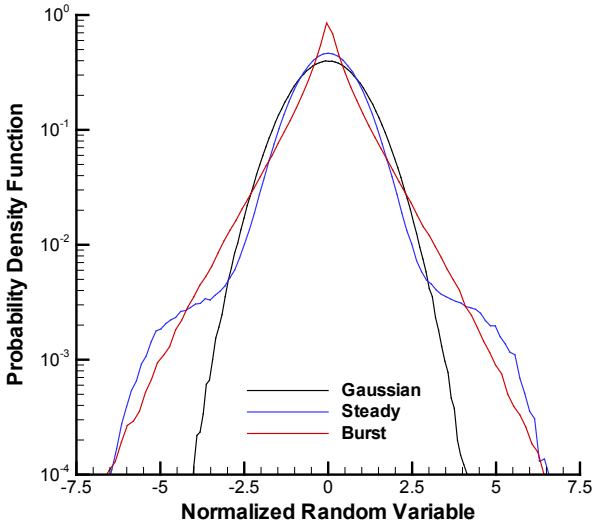

Figure 2. PDF of simulated Gaussian, and steady and burst non-Gaussian loadings.

4 LINEAR IMPULSE RESPONSE

Before embarking on the random response, the period L of the linear impulse response function was determined as a function of damping. The beam was subject to a 1 ms duration triangular pulse from an at-rest state. The response was simulated using the ABAQUS/Explicit solution. Figure 4 shows the displacement time history for the 0.25% damping condition. From this plot, the period of the impulse response can be seen to be about 5 s. The period of the impulse response for the 2% damping condition is roughly 1 s (not shown).

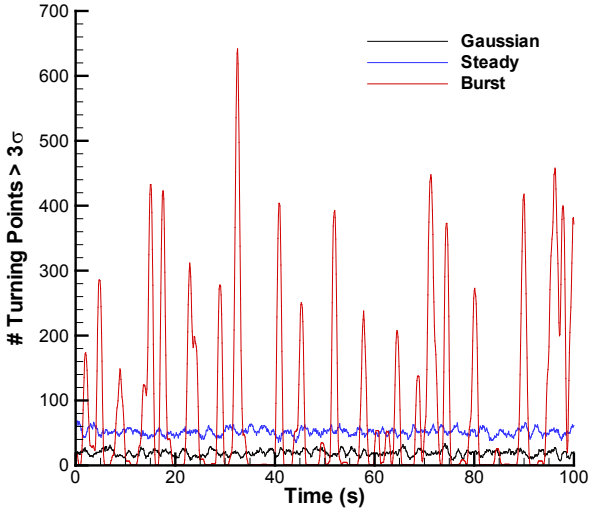

Figure 3. Turning point time history from simulated Gaussian, and steady and burst non-Gaussian loadings.

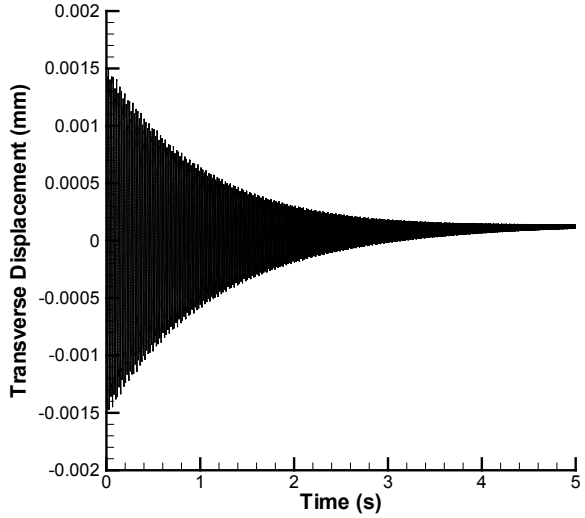

Figure 4. Impulse response of the beam (ζ =0.25%).

5 LINEAR RANDOM RESPONSE

The linear response regime is next considered using the low level 104 dB loading. These results will aid in the interpretation of the nonlinear response to follow.

5.1 Gaussian Loading – Linear Response

The time history of the transverse displacement response due to the Gaussian loading is shown in the lower plot of Figure 5 for the 0.25% damping condition. The PSD in Figure 6 clearly shows the resonant nature of the response. Four symmetric bending modes contributed to the response in the excitation bandwidth.

The PDF of the transverse displacement response is shown in Figure 7 for both levels of damping. Also plotted are the Gaussian PDFs, computed from equation (1) using the respective standard deviations and (zero) means. The expected near-Gaussian response is reflected in the computed kurtosis values of 3.01 and 2.90 for damping factors of 0.25% and 2%, respectively. As expected, the more lightly damped condition has greater displacement amplitudes.

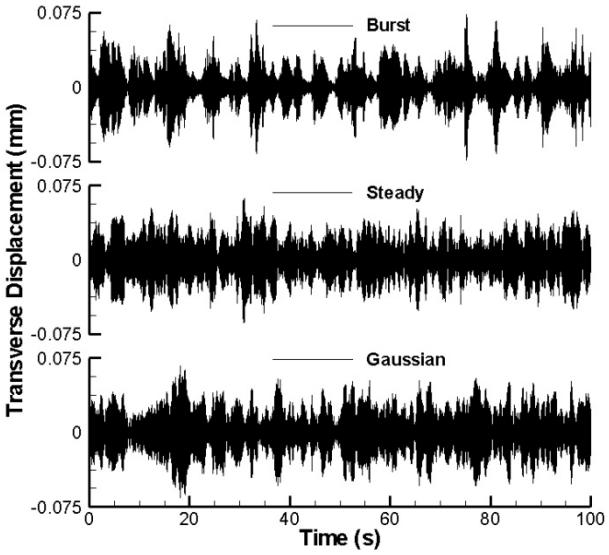

Figure 5. Time history of transverse displacement response due to three random loadings (ζ =0.25%).

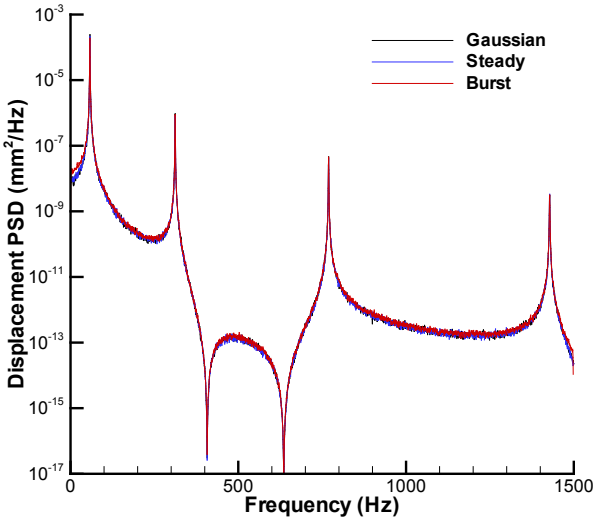

Figure 6. Linear displacement response PSD for Gaussian, and steady and burst non-Gaussian loadings (ζ =0.25%).

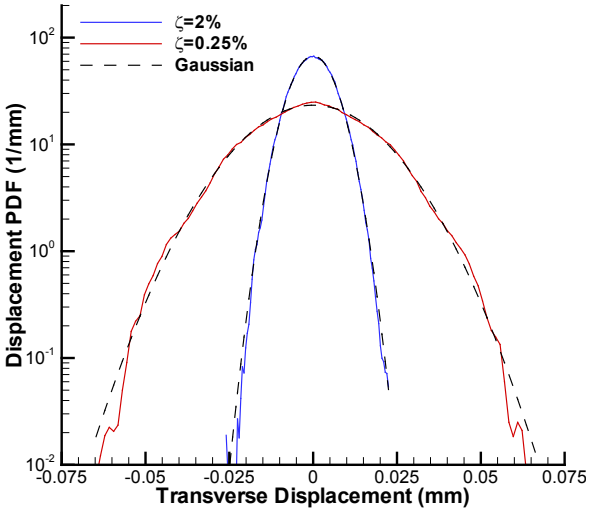

Figure 7. Linear transverse displacement response PDF due to a Gaussian loading.

5.2 *Steady Non-Gaussian Loading – Linear Response*

The displacement time history due to the steady non-Gaussian loading is shown in the middle plot of Figure 5. Its character is similar to the displacement response due to the Gaussian loading. The PSD and PDF are shown in Figure 6 and in Figure 8, respectively. Despite the fact that the excitation is non-Gaussian (γ =7.11), the PDFs are nearly identical, in both shape and magnitude, to the Gaussian loading case, with kurtosis values of 2.82 and 2.93 for damping factors of 0.25% and 2%, respectively.

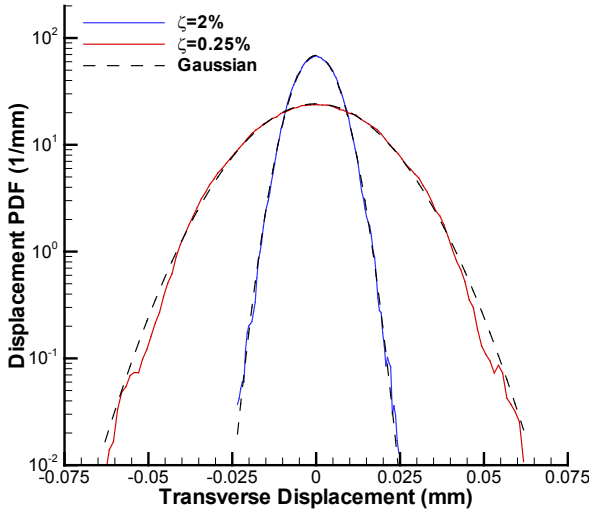

Figure 8. Linear transverse displacement response PDF due to a steady non-Gaussian loading.

The insensitivity of the response PDF to the non-Gaussian excitation can be explained in terms of the CLT. For either level of damping, the period of the system impulse response is much greater than the rate of peaks in the loading, about 50 per second. Thus, the displacement (sum random variable) at any time is not heavily weighted by a few terms in the sum because the convolution process averages out peak values. Since all the other conditions of the CLT have been met, the displacement distribution is Gaussian.

5.3 *Burst Non-Gaussian Loading – Linear Response*

The top plot of Figure 5 shows the displacement response due to the burst non-Gaussian loading. Its features more closely resemble that of the loading shown in Figure 1. While the response PSD is virtually identical to the previous loadings (see Figure 6), the PDFs are not. Figure 9 shows the response to be non-Gaussian for both levels of damping. In each case, wider tails and sharper peaks are shown relative to the corresponding Gaussian PDFs with the same standard deviation and (zero) mean.

The fact that the PDF is non-Gaussian can again be explained by the CLT. For the burst non-Gaussian loading, the timescale associated with each burst is on the order of 1-2 s, see Figure 1. The burst timescale is comparable to that of the impulse response period. Consequently, the convolution at any output time may be significantly weighted by a few terms, in violation of a requirement of the CLT. Accordingly, the distribution of the sum random variable is not Gaussian.

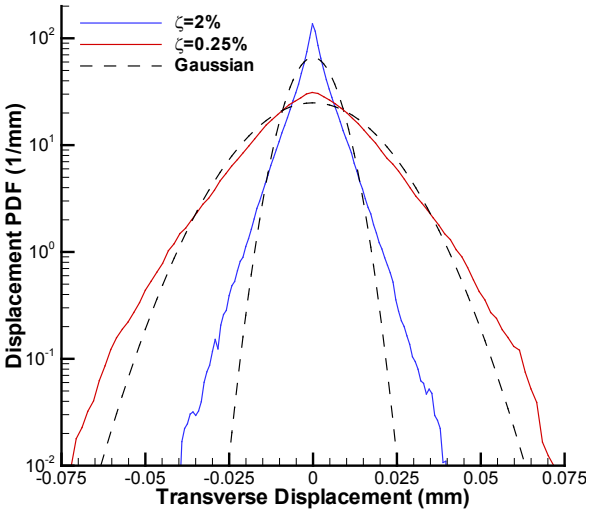

Figure 9. Linear transverse displacement response PDF due to a non-Gaussian burst loading.

While the CLT can give an indication if the response distribution tends toward Gaussian, it cannot be used to describe the shape if non-Gaussian. For the linear system, the shape is dependent on the damping. The lower damping condition resulted in a kurtosis of 3.95 while the higher damping condition had a kurtosis of 6.16. To help understand the relationship between the damping level and response kurtosis, it is useful to examine the time history response. Shown in Figure 10 is a close-up view of the displacement response for two levels of damping following a burst in the loading between 10.5 and 11.5 s. The magnitudes have been normalized to facilitate the comparison. The more highly damped system is shown to generally follow the loading envelope. In contrast, the lightly damped system behaves as if it is in free vibration following a loading burst. It was shown in Section 4 that the period of the impulse response function becomes shorter as damping is increased. The convolution of a short impulse response with the burst random loading will give a response that is heavily weighted by the most recent loading, see equation (7). In other words, the response closely follows the loading when the damping is high. For a more lightly damped system, the longer impulse response lessens this weighting and allows the system to ring when the loading rapidly decreases.

The ringing manifests itself in a lower kurtosis by allowing the system to respond for a longer time at the extreme values. The PDF of the free vibration response is shown in Figure 11 for varying amounts of damping. As the damping factor is reduced from 2% to 0.25%, the displacement PDF progresses from one that is primarily unimodal in character to one that is more bimodal in character. In the process, the kurtosis is reduced from 2.88 to 1.52. In the limit of near zero damping, the response PDF is highly bimodal and the kurtosis reaches a lower limit of 1.5. The lower damping thus gives rise to a lower response kurtosis under the burst non-Gaussian loading. The amount that kurtosis is lowered is proportional to the fractional duration of the ringing. Evidence of this bimodal character can be seen in the PDF of the 0.25% damping condition at a displacement of roughly ±0.062 mm, see Figure

9. This feature is not as prominent as in Figure 11 because a significant portion of the beam response is still forced.

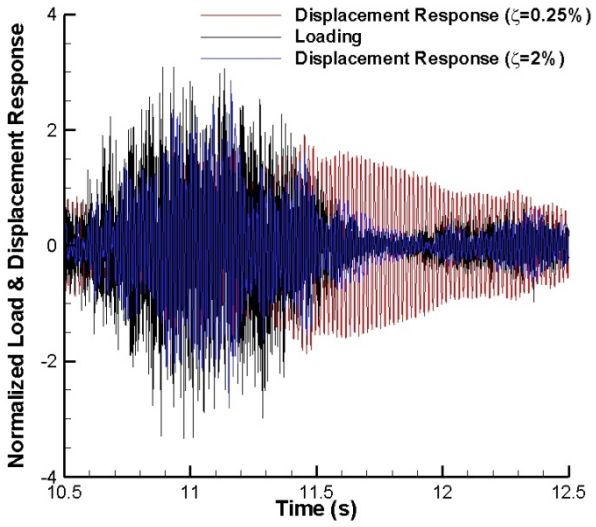

Figure 10. Time history of displacement response for two levels of damping for burst non-Gaussian loading.

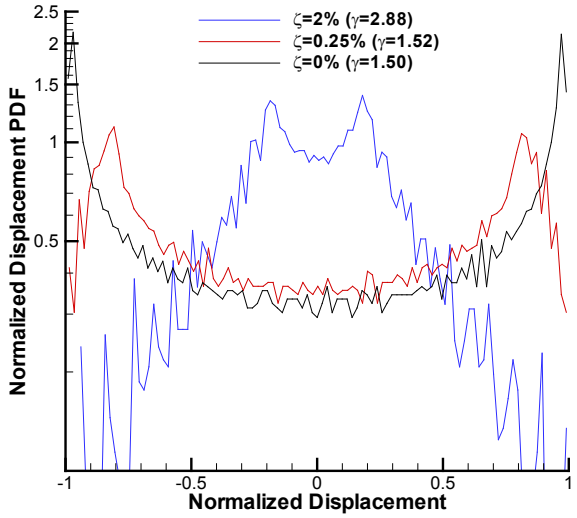

Figure 11. Displacement PDF of free vibration response with varying amounts of damping.

6 NONLINEAR RANDOM RESPONSE

The displacement response for a geometrically nonlinear response regime was simulated using the higher level 152 dB loading. The higher loading level is 256 times the pressure used to simulate the linear response. The loading distribution, simulation times, and post-processing were the same as used for the linear response regime results. Note that for each of the three loading types, the specified mass proportional damping constant c was unchanged between linear and nonlinear excitation levels

6.1 Gaussian Loading – Nonlinear Response

The displacement response time histories due to the Gaussian loading are shown in the bottom plot of Figure 12 for the 0.25% damping conditions. The red trace shows the nonlinear response while the black trace shows the linear response scaled by 256. The effect of a spring-hardening type nonlinearity is indicated by the reduced amplitude of the nonlinear response. Compared to Figure 6, the PSD shown in Figure 13 is clearly nonlinear, with broadening of peaks and shifting to higher frequencies, again a characteristic of a spring-hardening type of nonlinearity.

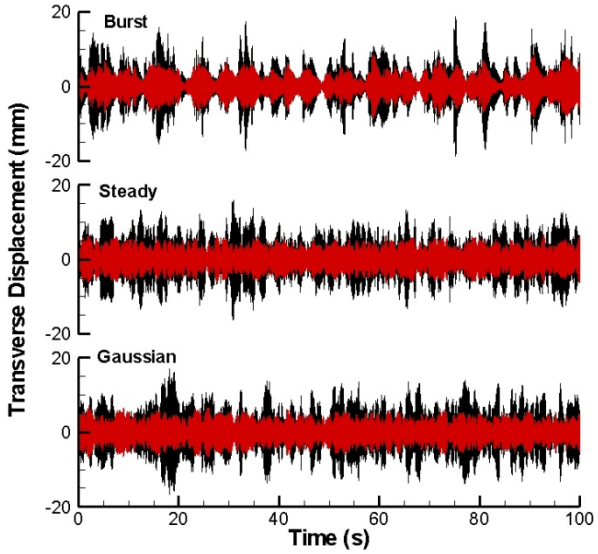

Figure 12. Time history of transverse displacement response due to three random loadings (ζ =0.25%). [Nonlinear response in red, scaled linear response in black].

The displacement response PDF, shown in Figure 14, is seen to be non-Gaussian for both damping conditions. This can again be explained as a violation of a condition of the CLT. Specifically, the coefficients h_i used in the summed random variable are required to be fixed constants, see equation (4). For the nonlinear system, the coefficients can no longer be considered as the impulse response. Nevertheless, in order for the sum random variable to represent the displacement, the coefficients would need to be amplitude dependent, not constant. As such, the CLT is violated and the PDFs for all the nonlinear displacement responses are non-Gaussian.

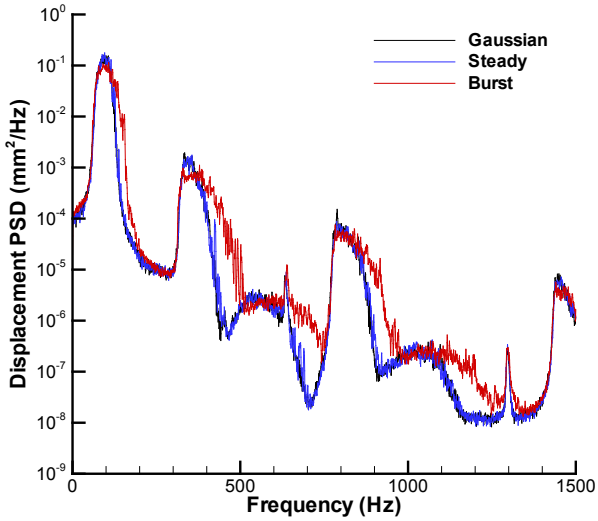

Figure 13. Nonlinear displacement PSD for Gaussian, and steady and burst non-Gaussian loadings (ζ =0.25%).

As previously indicated, the CLT does not indicate the shape of the PDF when violated. For the nonlinear system, the shape is a function of the nonlinearity and the damping. For a spring-hardening nonlinearity, the kurtosis is reduced relative to the linear response because the extreme values, shown in Figure 12, are attenuated, causing a narrowing of the tails of the PDF, see Figure 14. There is a greater degree of nonlinearity for the lower damping condition because of the increased amplitudes associated with its response. Therefore, the 0.25% damping condition has a lower kurtosis, but still higher amplitude, than the 2% damping condition; 2.33 versus 2.56. Note that other nonlinearities would exhibit other behaviors. For example, for a nonlinear system exhibiting only spring-softening behavior, the extreme values would increase relative to the linear response and hence the kurtosis would increase. For a nonlinear system in a thermally post-buckled condition [1, 2], a non-zero skewness would make the response non-Gaussian. Demonstration of the latter two nonlinear responses is outside the scope of this work.

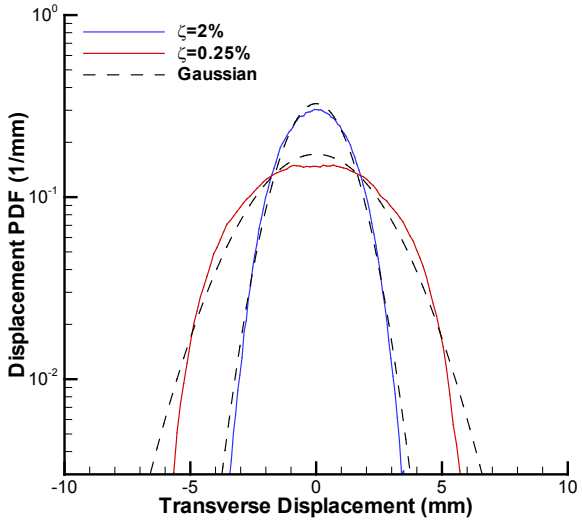

Figure 14. Nonlinear transverse displacement response PDF due to a Gaussian loading.

6.2 Steady Non-Gaussian Loading – Nonlinear Response

As for the Gaussian loading, the displacement time history for the steady non-Gaussian loading indicates a spring-hardening nonlinearity, as shown in the middle plot of Figure 12. The response PSD shows the degree of nonlinearity to be comparable to the Gaussian loading case, see Figure 13. Therefore, kurtosis values are comparable to the Gaussian loading cases, 2.23 and 2.54 for the 0.25% and 2% damping conditions, respectively. The PDFs are very similar to those presented in Figure 14, and are omitted for brevity.

6.3 Burst Non-Gaussian Loading – Nonlinear Response

While not particularly evident in the displacement time history shown in the upper plot of Figure 12, the PSD for the non-Gaussian burst loading exhibits a greater degree of nonlinearity than the other loading conditions, as shown in Figure 13. This is seen by the increased broadening of the peaks and slightly reduced amplitudes. The PDF for the 2% damping condition still has a high kurtosis of 4.35, but is lower than the 6.16 observed in the linear case, see Figure 15. The kurtosis for the 0.25% damping condition is 2.82, indicating that the tails of the PDF are narrower than if the response was Gaussian.

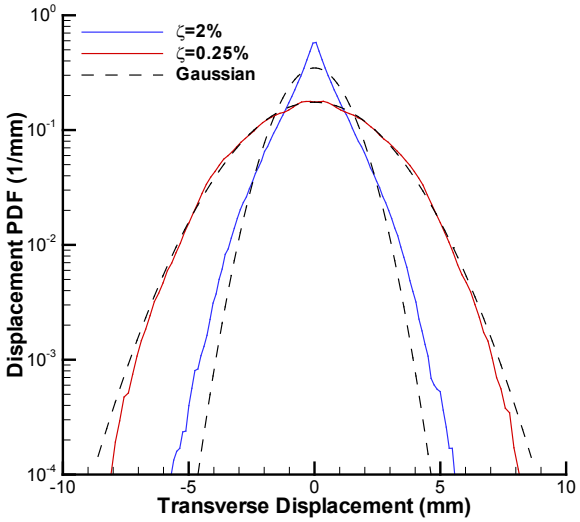

Figure 15. Nonlinear transverse displacement response PDF due to a burst random loading.

Finally, a comparison of the response time histories for both levels of damping, analogous to Figure 10, still indicates ringing behavior in the 0.25% damping condition response. The plot is not shown for brevity. Therefore, the lower kurtosis relative to the 2% damping condition is also, in part, due to this ringing behavior.

7 RELEVANCE TO RANDOM VIBRATION TESTING

The ability of a particular non-Gaussian loading to induce a non-Gaussian response has relevance not only to simulation, but also to testing. Recent developments in random vibration control allow simultaneous specification of not only the PSD and level, but also of the kurtosis [8-11]. The analyses presented in this paper relate to the efficacy of experimental methods developed to simulate high kurtosis loadings, the goals of which appear to be either for creating a more realistic simulation of the service loading, or for performing accelerated testing. With regard to the first goal, it was shown that the response PDF is Gaussian when the period of the system impulse response is much greater than the rate of peaks in the loading. In the linear response regime, this would appear to negate the need for high kurtosis random testing under such conditions. When the timescale of the loading peaks is comparable to the period of the impulse response, added damping would allow for greater kurtosis of the device under test, albeit at a reduced response level.

With regard to the second goal, kurtosis is manipulated to incur a greater response of the device under test in order to perform accelerated testing. This is essentially what was demonstrated numerically for the burst non-Gaussian loading relative to the Gaussian loading. Aside from the usual power limitations, the drive signal gain may also have to be limited to avoid a nonlinear structural response. If a spring-hardening nonlinearity is present, the kurtosis will decrease as demonstrated. Conversely, a spring-softening nonlinearity may be beneficial to achieving even higher kurtosis levels.

8 CONCLUSIONS

The response of a structure subject to Gaussian and non-Gaussian loadings in the linear and nonlinear response regimes was studied.

In the linear regime, it was found that non-Gaussian loadings produced Gaussian responses when the period of the system impulse response is much greater than the rate of peaks in the loading. This response distribution was shown to be a consequence of the Central Limit Theorem. Under this condition, the response was insensitive to the range of damping considered. When the timescale of peaks in the loading is comparable or greater than the period of the system impulse response, the CLT was violated and the response was non-Gaussian. Under this condition, low damping allowed ringing in the response, resulting in lower kurtosis.

In the nonlinear regime, all responses were non-Gaussian because the CLT requirement was violated by the amplitude dependent stiffness of the system. The effect of a spring-hardening type of nonlinearity was found to limit extreme values and thereby lower the kurtosis relative to the linear response regime. The level of damping affected the response kurtosis by affecting the degree of nonlinear stiffening. Additional work is needed to characterize the effect of other nonlinear mechanisms.

Finally, observations for high kurtosis random vibration testing were made including when such testing may be required, and how nonlinearities affect the ability to achieve high kurtosis values.

REFERENCES

[1] Przekop, A., Rizzi, S.A., and Sweitzer, K.A., "An investigation of high-cycle fatigue models for metallic structures exhibiting snap-through response," *International Journal of Fatigue*, Vol. 30, No. 9, pp. 1579-1598, 2008.

[2] Rizzi, S.A., Behnke, M.N., and Przekop, A., "The effect of a non-Gaussian random loading on high-cycle fatigue of a thermally post-buckled structure," *Structural Dynamics: Recent Advances, Proceedings of the 10th International Conference*, Paper 26, Southampton, UK, July 12-14, 2010.

[3] Steinwolf, A. and Rizzi, S.A., "Non-gaussian analysis of turbulent boundary layer fluctuating pressure on aircraft skin panels," *AIAA Journal of Aircraft*, Vol. 43, No. 6, pp. 1662-1675, 2006.

[4] Bendat, J.S. and Piersol, A.G., *Random data: Analysis and measurement procedures*, Wiley-Interscience, 1971.

[5] "ABAQUS online documentation, ABAQUS analysis user's manual." Providence, RI: Dassault Systemes Simulia Corp., 2009.

[6] Smallwood, D.O., "Vibration with non-Gaussian noise," *Journal of the Institute of Environmental Sciences and Technology*, Vol. 52, No. 3, pp. 13-30, 2009.

[7] "WAFO - A Matlab toolbox for analysis of random waves and loads," Version 2.1.1, The WAFO Group, Lund Institute of Technology, Lund University, 2005.

[8] Steinwolf, A., "Shaker simulation of random vibrations with a high kurtosis value," *Journal of the Institute of Environmental Sciences*, Vol. XL, No. 3, pp. 33-43, 1997.

[9] Steinwolf, A., "Two methods for random shaker testing with low kurtosis," in *Sound & Vibration*, October 2008, pp. 18-22.

[10] Steinwolf, A., "Random vibration testing with crest factor limiting by kurtosis manipulation," *Experimental Techniques*, Vol. 34, No. 5, pp. 16-24, 2010.

[11] Minderhoud, J. and Van Baren, P., "Using Kurtosion to accelerate structural life testing," in *Sound & Vibration*, October 2010, pp. 8-12.